

ORIGINAL ARTICLE

***In Silico* Screening Of N-Ethylidene-4-(Furan-2-Yl) Oxazol-2-Amine Derivatives by Computational Analysis as Potential Murg-Glycosyltransferase Inhibitors for Bacterial Infection**

Kiran P. Sabale¹, Gopal K. Kakade²

¹ Department of Chemistry, Arts & Commerce College, Warwat Bakal, Sangrampur, Buldhana, Maharashtra, India

² Department of Chemistry, Rajmata Jijau Mahavidyalaya, Kille Dharur, Dharur, Beed, Maharashtra India.

Corresponding Author Email: kpsabale1@gmail.com; **ORCID:**0009-0002-5008-8664

ABSTRACT

The limited success of conventional antibiotics against resistant pathogens has emphasized the need for novel antibacterial strategies. MurG-glycosyltransferase, a key enzyme in peptidoglycan biosynthesis, represents a promising but underexplored target. In this work, twenty N-ethylidene-4-(furan-2-yl)oxazol-2-amine derivatives were computationally designed and evaluated as potential MurG inhibitors. The ligands were energy-minimized and subjected to molecular docking using AutoDock Vina (PDB ID: 1NLM), while pharmacokinetic and toxicity properties were predicted through SwissADME and ADMETlab 3.0. Docking simulations revealed favorable binding affinities for several derivatives compared to the native ligand, with KS16 achieving the highest docking score (–8.9 kcal/mol), followed by KS20, KS10, and KS15. Interaction profiling showed consistent hydrogen bonding, electrostatic attraction, and hydrophobic stabilization with key active-site residues including GLU269, ARG164, and PHE21, supporting strong complementarity between the designed scaffolds and MurG. ADMET analysis further indicated that multiple derivatives, notably KS7, KS8, KS12, and KS20, demonstrated improved drug-likeness, oral absorption, and bioavailability predictions over the reference compound. Together, these computational findings identify several N-ethylidene-4-(furan-2-yl)oxazol-2-amine derivatives with favorable pharmacological profiles and MurG inhibitory potential. This study highlights their promise as lead scaffolds for antibacterial development and provides a foundation for subsequent experimental evaluation.

Keywords: MurG-glycosyltransferase, antibacterial, ADMET, molecular docking

Received 12.04.2025

Revised 15.07.2025

Accepted 19.08.2025

How to cite this article:

Kiran P. S, Gopal K. K. *In Silico* Screening of N-Ethylidene-4-(Furan-2-Yl) Oxazol-2-Amine Derivatives by Computational Analysis as Potential Murg-Glycosyltransferase Inhibitors for Bacterial Infection. Adv. Biores., Vol 16 (5) September 2025: 66-85.

INTRODUCTION

Bacterial infections continue to be a major global health concern, contributing to significant morbidity and mortality despite decades of progress in antimicrobial therapy [1,2]. The emergence and rapid spread of antimicrobial resistance (AMR) have substantially reduced the effectiveness of conventional antibiotics, creating an urgent need for novel therapeutic strategies [3]. According to the World Health Organization, resistant bacterial pathogens pose one of the greatest threats to public health in the 21st century, with multidrug-resistant (MDR) strains complicating treatment outcomes and leading to prolonged illness, higher medical costs, and increased mortality. The limited availability of new antibiotics, together with the persistent emergence of resistance strains, demands the investigation of alternate strategies to discover new therapeutic targets and inhibitors with innovative modes of action. Among the potential bacterial pathways, the peptidoglycan biosynthesis process has emerged as a highly promising target, owing to its essential role in bacterial cell wall formation and its absence in human metabolic pathways [4–7].

Peptidoglycan is a crucial structural component of the bacterial cell wall, providing rigidity and protecting cells from osmotic lysis. Its biosynthesis involves a highly coordinated series of enzymatic steps, many of

which are indispensable for bacterial survival and growth [8–11]. One such critical enzyme is MurG-glycosyltransferase, which catalyzes the final intracellular step of peptidoglycan precursor synthesis. Specifically, MurG facilitates the transfer of N-acetylglucosamine (GlcNAc) to lipid I, forming lipid II, a universal precursor for cell wall biosynthesis in both Gram-positive and Gram-negative bacteria. Inhibition of MurG effectively blocks cell wall formation, leading to bacterial death. Unlike several other peptidoglycan biosynthesis enzymes that already serve as targets for existing antibiotics, MurG remains underexplored, making it a particularly attractive target for the development of next-generation antibacterial agents [12–16].

In recent years, computational approaches such as molecular docking, pharmacokinetic profiling, and virtual screening have emerged as powerful tools in early-stage drug discovery. These methods allow rapid, cost-effective evaluation of large chemical libraries to identify potential drug candidates before experimental validation. *In silico* screening not only accelerates the drug discovery process but also enhances target-specificity predictions by providing structural and mechanistic insights into ligand-protein interactions. By concentrating on critical binding sites of target proteins, computational techniques reduce attrition rates in subsequent experimental phases and promote rational drug design [17–20].

The search for effective MurG inhibitors has motivated the exploration of novel heterocyclic compounds, which are well-recognized for their diverse biological activities and structural versatility [21,22]. Among heterocyclic frameworks, oxazole and furan scaffolds have been widely studied in medicinal chemistry due to their antimicrobial, anticancer, and anti-inflammatory potentials. The incorporation of oxazole moieties often enhances bioactivity through favorable hydrogen-bonding interactions with target proteins, while furan rings contribute to aromatic stacking and electron-rich interactions that stabilize ligand-enzyme complexes. Furthermore, Schiff base derivatives, formed through condensation reactions of primary amines with carbonyl compounds, have gained attention due to their pharmacological diversity, metal-chelating ability, and high binding affinity toward various biomolecular targets.

In this context, N-ethylidene-4-(furan-2-yl)oxazol-2-amine derivatives represent a rationally designed class of compounds combining oxazole and furan scaffolds with Schiff base characteristics. Such hybrid structures are anticipated to exhibit improved antibacterial potency by leveraging multiple pharmacophoric features capable of interacting with MurG active sites. However, the potential of these compounds as MurG inhibitors has not to be comprehensively assessed. Computational analysis of their binding affinity, stability, and pharmacokinetic properties offers a strategic starting point for identifying lead molecules for further *in vitro* and *in vivo* studies.

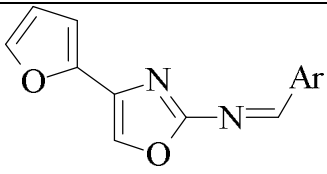
The present study aims to perform an *In silico* screening of N-ethylidene-4-(furan-2-yl)oxazol-2-amine derivatives as potential MurG-glycosyltransferase inhibitors for bacterial infection management. Through molecular docking, binding energy calculations, and pharmacokinetic predictions, this research seeks to identify compounds with high inhibitory potential, favorable ADMET properties, and stable interaction profiles within the MurG active site. The outcomes of this study will provide critical insights into the design of novel antibacterial agents targeting MurG and contribute to the ongoing efforts to combat antimicrobial resistance through the discovery of innovative chemotherapeutic agents.

MATERIAL AND METHODS

Molecules Designing and Ligand Preparation

All N-ethylidene-4-(furan-2-yl)oxazol-2-amine derivatives were designed using ChemDraw Ultra, and their 2D structures were converted into 3D using Chem3D. The ligands were energy-minimized and saved in MOL format for computational analysis. Structural modifications and substituents incorporated for derivative design are illustrated in Table 1.

Table 1: The structure of all selected substitutions and parent nucleus.

 <p>N-ethylidene-4-(furan-2-yl)oxazol-2-amine derivative (1-20)</p>			
Compound Code	Substitutions	Compound Code	Substitutions

KS1	—2-pyridyl	KS11	—3-hydroxy phenyl
KS2	—phenyl	KS12	—2,3,4-trihydroxy phenyl
KS3	—4-nitro phenyl	KS13	—3-methoxy-4-hydroxy phenyl
KS4	—4-bromo phenyl	KS14	—2-methoxy phenyl
KS5	—4-fluoro phenyl	KS15	—4-styryl
KS6	—4-chloro phenyl	KS16	—naphthyl
KS7	—4-methyl phenyl	KS17	—2,4-dinitro phenyl
KS8	—4-methoxy phenyl	KS18	—4-methylsulfonyl phenyl
KS9	—4-hydroxy phenyl	KS19	—4-dimethylamino phenyl
KS10	—3-nitro phenyl	KS20	—4-trifluoromethyl phenyl

***In silico* ADMET Screening**

In drug development, *in silico* ADMET screening plays a crucial role in the early identification of potential pharmacokinetic and toxicity issues. This computational approach enables scientists to simulate drug behavior in the human body, thereby reducing the likelihood of late-stage failures, minimizing time requirements, and decreasing costs associated with experimental testing. Consequently, this process accelerates the development of new medications and enhances the probability of achieving safe and effective therapies [23]. To assess ADMET parameters in this study, two platforms were utilized: ADMETlab 3.0 and SwissADME. ADMETlab 3.0, the latest iteration of this platform, offers a comprehensive and efficient system for analyzing ADMET metrics, physicochemical properties, and key medicinal chemistry characteristics pertinent to drug design. SwissADME complements this by providing calculations for physicochemical descriptors and predictions for ADME characteristics, pharmacokinetic properties, drug-likeness, and medicinal chemistry suitability for single or multiple small molecules. The combined use of these tools significantly enhances the drug development process [24–28].

Molecular Docking

We performed molecular docking analyses using AutoDock Vina 1.2.0. The crystal structure of MurG-glycosyltransferase (PDB ID: 1NLM) was obtained from the Protein Data Bank (<https://www.rcsb.org/structure/4y6m>) and processed using AutoDockTools 1.5.6. Water molecules were removed, polar hydrogen atoms were added, and Gasteiger charges were assigned. Ligands were constructed using OpenBabel 3.1.1 to generate three-dimensional structures and optimize energy levels. The grid box was centered on the active site at coordinates X: 37.884282, Y: -3.588333, and Z: 20.849103. The highest-scoring poses were selected based on binding affinity and protein-ligand interactions [23,29]. All ligands, including the native ligand and target, were input into the PyRx virtual screening program for docking experiments. After molecular docking we perform a docking interactions. These interactions were analyzed using Biovia Discovery Studio [24,30,31]. Figure 1 shows all the selected compounds along with the native ligand (NL) bound to the MurG-glycosyltransferase enzyme (PDB ID: 1NLM).

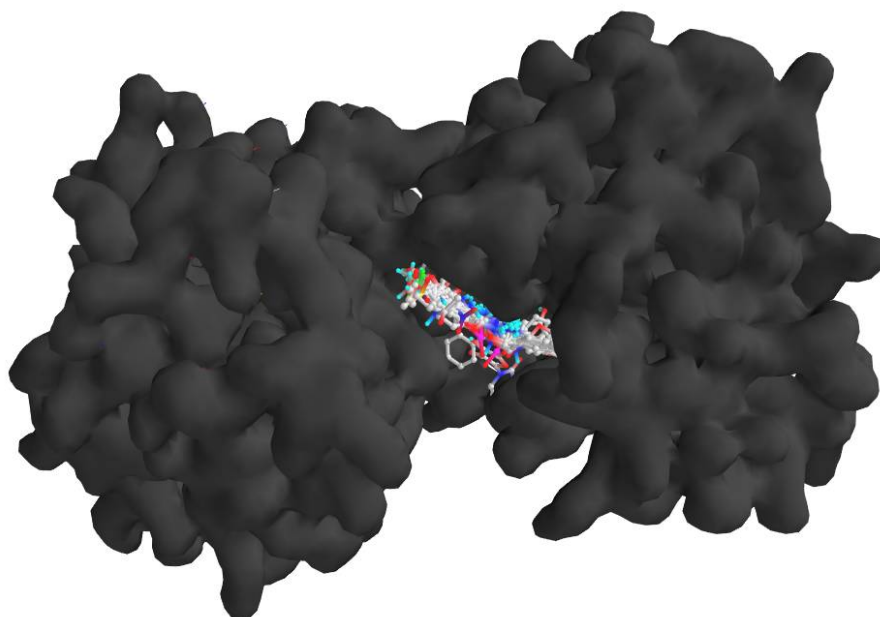


Figure 1: Molecular docking of all selected compounds and NL with MurG-glycosyltransferase enzyme (PDB ID: 1NLM).

RESULTS AND DISCUSSION

In Silico ADMET Analysis

ADMET (Absorption, Distribution, Metabolism, Excretion, and Toxicity) analysis is crucial in drug discovery and development, providing insights into a compound's behavior within biological systems. This *in silico* approach predicts pharmacokinetic and toxicological properties, helping to identify potential drug candidates and reduce the likelihood of late-stage failures. The analysis of the selected derivatives reveals significant variations in physicochemical properties compared to the native ligand (Table 2). The native ligand exhibits a higher molecular weight (607.08) and volume (488.45) than all derivatives, suggesting potential challenges in oral bioavailability. KS17 demonstrates the highest topological polar surface area (TPSA) among derivatives (137.81), indicating improved water solubility but possible limitations in membrane permeability. Lipophilicity (logP) values for all derivatives are generally lower than the native ligand (-3.32266), with KS16 showing the highest (4.223495), potentially enhancing membrane penetration. Notably, KS1 displays the lowest molecular weight (239.07) and volume (237.21), which may contribute to improved oral absorption. The number of hydrogen bond donors and acceptors varies among compounds, with KS17 and KS18 exhibiting the highest values, potentially affecting their ability to cross biological membranes. Overall, these derivatives present diverse physicochemical profiles, with several compounds showing promising characteristics for drug-like properties compared to the native ligand, warranting further investigation into their pharmacokinetic behavior and potential therapeutic applications. The ADMET radar of all selected compound and native ligand are shown in Table 8.

Table 2: Physicochemical properties of selected derivatives

Compounds	MW	Volume	Dense	nHA	nHD	nRot	nRing	TPSA	logS	logP
Native Ligand	607.08	488.4516	1.242866	20	8	11	3	294.86	0.143502	-3.32266
KS1	239.07	237.214	1.007824	5	0	3	3	64.42	-3.26016	2.60299
KS2	238.07	243.5132	0.977647	4	0	3	3	51.53	-4.19996	3.206622
KS3	283.06	269.4539	1.050495	7	0	4	3	94.67	-4.82537	2.961508
KS4	315.98	262.7968	1.202374	4	0	3	3	51.53	-5.08397	3.99329
KS5	256.06	249.5807	1.025961	4	0	3	3	51.53	-4.18481	3.248798
KS6	272.04	258.7242	1.051467	4	0	3	3	51.53	-5.04988	3.970746
KS7	252.09	260.8092	0.966569	4	0	3	3	51.53	-4.85529	3.816114
KS8	268.08	269.5994	0.994364	5	0	4	3	60.76	-4.43798	3.117477
KS9	254.07	252.3034	1.007002	5	1	3	3	71.76	-3.76912	2.728667
KS10	283.06	269.4539	1.050495	7	0	4	3	94.67	-4.73924	3.041798
KS11	254.07	252.3034	1.007002	5	1	3	3	71.76	-4.03919	2.9815
KS12	286.06	269.8839	1.059937	7	3	3	3	112.22	-3.92949	2.421738
KS13	284.08	278.3896	1.02044	6	1	4	3	80.99	-4.00378	2.46745
KS14	268.08	269.5994	0.994364	5	0	4	3	60.76	-4.49018	3.419037
KS15	264.09	275.4687	0.958693	4	0	4	3	51.53	-4.16289	3.805061
KS16	288.09	298.8677	0.963938	4	0	3	4	51.53	-5.09606	4.223495
KS17	328.04	295.3947	1.110514	10	0	5	3	137.81	-4.7564	2.934022
KS18	316.05	296.8986	1.064505	6	0	4	3	85.67	-3.94756	2.240795
KS19	281.12	289.1019	0.972391	5	0	4	3	54.77	-4.43781	3.325567
KS20	306.06	279.0118	1.096943	4	0	4	3	51.53	-5.03459	4.029549

Drug-likeness is a crucial concept in drug discovery that assesses the likelihood of a compound becoming an orally active drug in humans. It encompasses various physicochemical properties that influence a compound's behavior in the body. As shown in Table 3, the drug-likeness properties of the designed derivatives were evaluated using multiple parameters and rules. Comparing the results to the native ligand, it is evident that most of the designed compounds exhibit improved drug-like characteristics. The native ligand has a low QED score of 0.117, while the majority of the derivatives show significantly higher QED values, ranging from 0.397 to 0.742. Notably, compounds KS9, KS11, and KS13 demonstrate the highest QED scores (0.727, 0.727, and 0.742, respectively), indicating enhanced drug-likeness. The NP

scores for the derivatives are generally lower than the native ligand, suggesting better synthetic accessibility. Regarding compliance with various drug-likeness rules, the native ligand violates the Lipinski, Pfizer, and GSK rules, whereas many derivatives show improved compliance. For instance, compounds KS1, KS3, KS17, and KS18 satisfy all the evaluated rules, potentially indicating better pharmacokinetic properties. However, it is important to note that some compounds, such as KS3, KS10, and KS17, have lower QED scores, which may require further optimization. Overall, the designed derivatives demonstrate promising drug-like properties compared to the native ligand, with several compounds showing potential for further development in drug discovery efforts.

Table 3: Drug-likeness properties of designed derivatives

Compounds	QED	NP Score	Lipinski Rule	Pfizer Rule	GSK Rule	GoldenTriangle	Chelator Rule
Native Ligand	0.117	1.051	1	0	1	1	0
KS1	0.659	-1.488	0	0	0	0	0
KS2	0.654	-1.235	0	1	0	0	0
KS3	0.414	-1.561	0	0	0	0	0
KS4	0.671	-1.335	0	1	0	0	0
KS5	0.669	-1.596	0	1	0	0	0
KS6	0.667	-1.478	0	1	0	0	0
KS7	0.662	-1.331	0	1	0	0	0
KS8	0.677	-1.139	0	1	0	0	0
KS9	0.727	-0.852	0	0	0	0	0
KS10	0.414	-1.7	0	0	0	0	0
KS11	0.727	-0.842	0	0	0	0	0
KS12	0.504	-0.492	0	0	0	0	1
KS13	0.742	-0.618	0	0	0	0	1
KS14	0.677	-1.159	0	1	0	0	0
KS15	0.658	-0.753	0	1	0	0	0
KS16	0.507	-1.149	0	1	1	0	0
KS17	0.397	-1.501	0	0	0	0	0
KS18	0.69	-1.536	0	0	0	0	0
KS19	0.683	-1.419	0	1	0	0	0
KS20	0.659	-1.443	0	1	1	0	0

Absorption is a crucial pharmacokinetic parameter that determines the extent to which a drug enters the systemic circulation after administration. It is influenced by various factors, including the compound's ability to permeate through biological membranes and its interaction with efflux transporters. As shown in Table 4, the absorption parameters of the selected compounds were evaluated and compared to the native ligand. The Caco-2 and MDCK permeability values for all compounds, including the native ligand, were negative, indicating low permeability. However, most of the synthesized compounds (KS1-KS20) showed improved Pgp-inhibition and Pgp-substrate properties compared to the native ligand. Notably, compounds KS7, KS8, KS12, and KS19 demonstrated high Pgp-inhibition (>0.93) and Pgp-substrate (>0.98) values, suggesting their potential to overcome multidrug resistance. The human intestinal absorption (HIA) values for the majority of the compounds were higher than the native ligand, with KS7, KS8, KS12, KS15, and KS19 exhibiting values above 0.9. Furthermore, the oral bioavailability predictions (F20%, F30%, and F50%) for most compounds were superior to the native ligand, indicating enhanced potential for oral administration. These results suggest that the synthesized compounds, particularly KS7, KS8, KS12, and KS19, possess improved absorption characteristics compared to the native ligand, making them promising candidates for further drug development.

Table 4: Absorption parameter of selected compounds

Compounds	Caco-2 Permeability	MDCK Permeability	Pgp-inhibitor	Pgp- substrate	HIA	F20%	F30%	F50%
Native Ligand	-5.89769	-5.26322	5.25E-05	4.86E-08	0.406585	4.43E-05	0.969539	0.042976
KS1	-4.72113	-4.67573	0.285373	0.000446	0.014274	0.340943	0.567542	0.46264
KS2	-4.72923	-4.61214	0.91515	1.26E-05	0.005723	0.617341	0.767185	0.767324
KS3	-4.79413	-4.65658	0.756034	2.61E-06	0.001442	0.630664	0.771904	0.833861
KS4	-4.77447	-4.65018	0.889259	1.27E-06	0.012387	0.804976	0.938694	0.882463
KS5	-4.46876	-4.6187	0.944254	2.38E-06	0.014404	0.934386	0.948806	0.782766
KS6	-4.57736	-4.69297	0.878093	2.31E-06	0.013555	0.866476	0.934825	0.859336
KS7	-4.70425	-4.66745	0.963085	3.87E-06	0.020232	0.985269	0.981994	0.955087
KS8	-4.87475	-4.73741	0.933277	8.45E-07	0.164093	0.991728	0.993406	0.946038
KS9	-4.92321	-4.74015	0.818487	4.60E-05	0.011076	0.861668	0.914511	0.942882
KS10	-4.8112	-4.62892	0.502022	4.22E-06	0.000641	0.390023	0.534157	0.561791
KS11	-4.94822	-4.76127	0.035868	1.02E-05	0.001696	0.672848	0.594517	0.837579
KS12	-4.87947	-4.75458	0.171563	3.85E-05	0.038997	0.973602	0.983991	0.983363
KS13	-4.90764	-4.76218	0.884756	0.000108	0.007381	0.681138	0.639042	0.896118
KS14	-4.62771	-4.66779	0.874597	0.0007	0.046144	0.55791	0.660845	0.871769
KS15	-4.65945	-4.59304	0.817648	0.00636	0.004615	0.548392	0.71347	0.91224
KS16	-4.72997	-4.59968	0.745613	5.70E-05	0.007965	0.375677	0.855669	0.841951
KS17	-4.82016	-4.57982	0.032176	1.49E-05	0.000187	0.074804	0.269534	0.662609
KS18	-4.86621	-4.82126	0.519932	6.02E-07	0.007451	0.68989	0.818809	0.394019
KS19	-4.77409	-4.6737	0.991071	1.14E-05	0.026892	0.918514	0.953017	0.898192
KS20	-4.67848	-4.73037	0.995761	6.29E-06	0.006545	0.915609	0.907677	0.526286

Distribution and metabolism are crucial factors in determining the pharmacokinetic properties of drug candidates. The analysis of selected molecules reveals significant variations in their distribution and metabolic profiles compared to the native ligand. The native ligand exhibits low plasma protein binding (PPB) of 19.86%, while the KS compounds show substantially higher PPB values ranging from 93.17% to 98.68%. This increased protein binding may impact the compounds' bioavailability and distribution. The volume of distribution (VD) values for KS compounds are generally higher than the native ligand, suggesting improved tissue penetration. Blood-brain barrier (BBB) permeability, represented by logBB values, varies among the compounds, with some showing better CNS penetration potential than the native ligand. Metabolic stability, assessed through CYP enzyme interactions, demonstrates diverse profiles for the KS compounds. While the native ligand shows minimal CYP enzyme inhibition and substrate potential, several KS compounds exhibit stronger interactions with various CYP isoforms. For instance, KS1, KS2, and KS4 show high inhibitory potential for CYP1A2, CYP2C19, and CYP2D6, respectively. Some compounds, such as KS14 and KS16, display substrate potential for multiple CYP enzymes, which may influence their metabolic clearance. These findings, as presented in Table 5, highlight the complex interplay of distribution and metabolic factors among the investigated compounds, emphasizing the need for careful consideration of these parameters in further drug development efforts.

Table 5: Distribution and metabolism parameter of selected molecules

Compounds	Distribution				Metabolism									
	PPB %	VD	BBB	Fu	CYP1A2		CYP2C19		CYP2C9		CYP2D6		CYP3A4	
					Inhibitor	Substrate	Inhibitor	Substrate	Inhibitor	Substrate	Inhibitor	Substrate	Inhibitor	Substrate
Native Ligand	19.86 314	- 0.771 99	3.78 E-07	71.72 19	4.36 E-11	4.64 E-06	1.03 E-08	1.71 E-07	9.40 E-08	1.64 E-06	5.31 E-09	2.85 E-09	1.49 E-08	4.74 E-05
KS1	93.17 123	- 0.298 14	0.144 393	4.691 448	0.999 952	0.140 148	0.983 895	4.32 E-06	0.290 145	0.965 363	1.24 E-05	0.010 217	0.002 788	0.029 842
KS2	97.89 584	- 0.094 01	0.014 812	1.670 486	0.999 972	0.004 24	0.986 476	8.91 E-06	0.988 384	0.000 335	2.77 E-06	0.003 273	0.018 813	1.31 E-06
KS3	94.53 615	- 0.218 14	0.000 158	5.905 7	0.975 458	0.031 212	0.306 638	0.000 341	0.847 687	0.048 198	0.000 363	0.166 607	0.005 01	0.000 429
KS4	97.24 968	0.235 389	0.009 004	2.316 666	0.999 501	0.002 595	0.977 576	0.000 411	0.998 853	0.009 652	0.000 426	0.243 682	0.015 929	2.56 E-05
KS5	97.10 015	0.003 696	0.002 281	2.531 938	0.999 84	0.004 513	0.963 673	0.000 142	0.994 909	0.009 035	0.000 198	0.064 032	0.020 686	1.53 E-05
KS6	98.68 091	- 0.208 4	0.004 4	1.054 809	0.999 996	0.049 597	0.999 092	4.77 E-05	0.999 805	0.005 8	0.011 591	0.090 809	0.008 829	0.000 119
KS7	97.82 052	- 0.034 84	0.000 661	2.103 513	0.999 982	0.002 411	0.980 86	8.95 E-05	0.998 673	0.005 142	2.76 E-05	0.094 136	0.117 605	1.10 E-05
KS8	96.14 932	- 0.059 71	0.000 3	3.610 238	0.999 216	0.025 068	0.997 802	0.010 256	0.999 37	0.022 901	0.000 128	0.780 083	0.028 623	0.000 26
KS9	96.30 099	- 0.127 52	0.000 305	3.333 26	0.999 341	0.001 453	0.595 636	2.69 E-05	0.952 162	0.031 835	0.000 193	0.663 918	0.097 795	1.39 E-06
KS10	97.85 264	- 0.105 85	0.000 348	1.914 101	0.999 954	0.007 832	0.999 867	0.000 929	0.986 132	0.070 649	0.000 388	0.039 945	0.015 571	1.15 E-05
KS11	95.81 978	- 0.403 68	0.001 365	3.461 707	0.998 797	0.004 959	0.990 047	9.79 E-06	0.989 132	0.001 11	1.25 E-05	0.055 046	0.339 084	9.93 E-06
KS12	95.76 196	- 0.465 15	0.000 724	2.972 858	0.988 575	0.009 98	0.133 376	1.50 E-05	0.602 31	0.160 845	9.62 E-06	0.180 646	0.281 538	3.68 E-07
KS13	97.58 361	- 0.524 55	0.002 417	2.264 887	0.999 636	0.036 733	0.987 947	0.002 662	0.976 162	0.069 079	0.003 096	0.391 599	0.084 941	8.13 E-05
KS14	97.72 192	- 0.029 07	0.015 964	1.861 967	1	0.019 517	0.998 865	4.80 E-05	0.999 848	0.081 32	0.070 399	0.914 988	0.988 11	0.000 862
KS15	98.51 026	- 0.242 03	0.001 244	1.103 554	0.999 989	0.001 555	0.998 909	2.96 E-06	0.995 257	0.433 105	0.001 248	0.931 778	0.038 566	7.65 E-08
KS16	98.33 527	0.075 909	0.003 195	1.132 391	0.999 999	0.113 248	0.999 926	0.018 969	0.998 173	0.703 548	0.002 214	0.937 934	0.009 167	0.000 366
KS17	97.83 987	- 0.372 29	0.000 646	2.461 895	0.998 803	3.31 E-06	0.992 93	3.48 E-05	0.998 441	0.000 123	0.191 476	0.002 591	0.478 758	0.004 115
KS18	96.99 037	- 0.199 57	0.000 519	3.513 705	0.873 927	0.007 414	0.125 981	0.002 436	0.695 177	0.103 189	3.59 E-05	0.011 228	0.000 288	0.000 213
KS19	96.87 576	0.184 014	8.08 E-05	2.759 493	0.999 811	0.012 128	0.988 994	0.000 117	0.967 799	0.005 715	0.003 164	0.045 119	0.008 632	1.70 E-05
KS20	97.20 656	0.310 658	0.029 487	2.463 224	0.988 293	0.090 215	0.893 332	0.003 314	0.942 671	0.090 736	0.000 564	0.150 044	0.006 411	0.001 103

Excretion and toxicity are crucial factors in drug development, influencing a compound's safety profile and pharmacokinetic properties. The analysis of these parameters for the native ligand and 20 selected

compounds (KS1-KS20) reveals diverse outcomes across various toxicity endpoints and excretion metrics (Table 6). Comparing the compounds to the native ligand, notable differences emerge in plasma clearance (CL-plasma) and half-life (T1/2). The native ligand exhibits a low CL-plasma (0.893693) and a relatively long T1/2 (33.26746), while the KS compounds generally show higher CL-plasma values (ranging from 3.453985 to 9.570157) and shorter T1/2 (0.4205410 to 1.157932). This suggests potentially faster elimination of the KS compounds from the body. Regarding toxicity, the native ligand demonstrates a low probability of hepatotoxicity (H-HTD: 0.022324) and drug-induced liver injury (DILI: 0.999996), whereas the KS compounds show varied results, with some exhibiting higher hepatotoxicity risks. Mutagenicity (Ames Toxicity) is generally higher in the KS compounds compared to the native ligand, indicating a potential increase in genetic toxicity. Acute toxicity (Rat Oral Acute Toxicity) is lower in the native ligand (0.035818) compared to most KS compounds. The FDA Maximum Daily Dose (FDA MDD) values are generally lower for the KS compounds, suggesting potentially safer daily dosage limits. Skin sensitization, carcinogenicity, and eye corrosion probabilities vary among the compounds, with some KS compounds showing improved profiles compared to the native ligand. Respiratory toxicity is notably higher in several KS compounds, particularly KS1, KS17, and KS19, compared to the native ligand. These findings underscore the importance of carefully evaluating the excretion and toxicity profiles of potential drug candidates in comparison to the native ligand to optimize safety and efficacy in drug development.

Environmental toxicity is a critical concern in the development of new compounds, as it directly impacts ecosystems and human health. The environmental toxicity profile of designed molecules provides crucial information about their potential effects on various organisms and the environment. In this study, we analyzed the environmental toxicity of 20 designed compounds (KS1-KS20) in comparison to the native ligand using parameters such as bioconcentration factor (BCF), IGC50, LC50FM, and LC50DM (Table 7). The results indicate that all designed compounds exhibited higher BCF values than the native ligand, suggesting increased potential for bioaccumulation. Compound KS4 showed the highest BCF value of 1.998658, while KS17 and KS18 had the lowest values of 0.543772 and 0.542329, respectively. In terms of IGC50, all compounds demonstrated higher values compared to the native ligand, with KS16 having the highest value of 4.24241. The LC50FM and LC50DM values for the designed compounds were generally higher than the native ligand, indicating potentially lower acute toxicity. Notably, KS6 exhibited the highest LC50FM and LC50DM values of 5.184766 and 5.665054, respectively. Overall, while the designed compounds showed improved environmental toxicity profiles in some aspects, their higher BCF values suggest the need for further optimization to reduce bioaccumulation potential.

Table 6: Excretion and Toxicity parameters of selected compounds

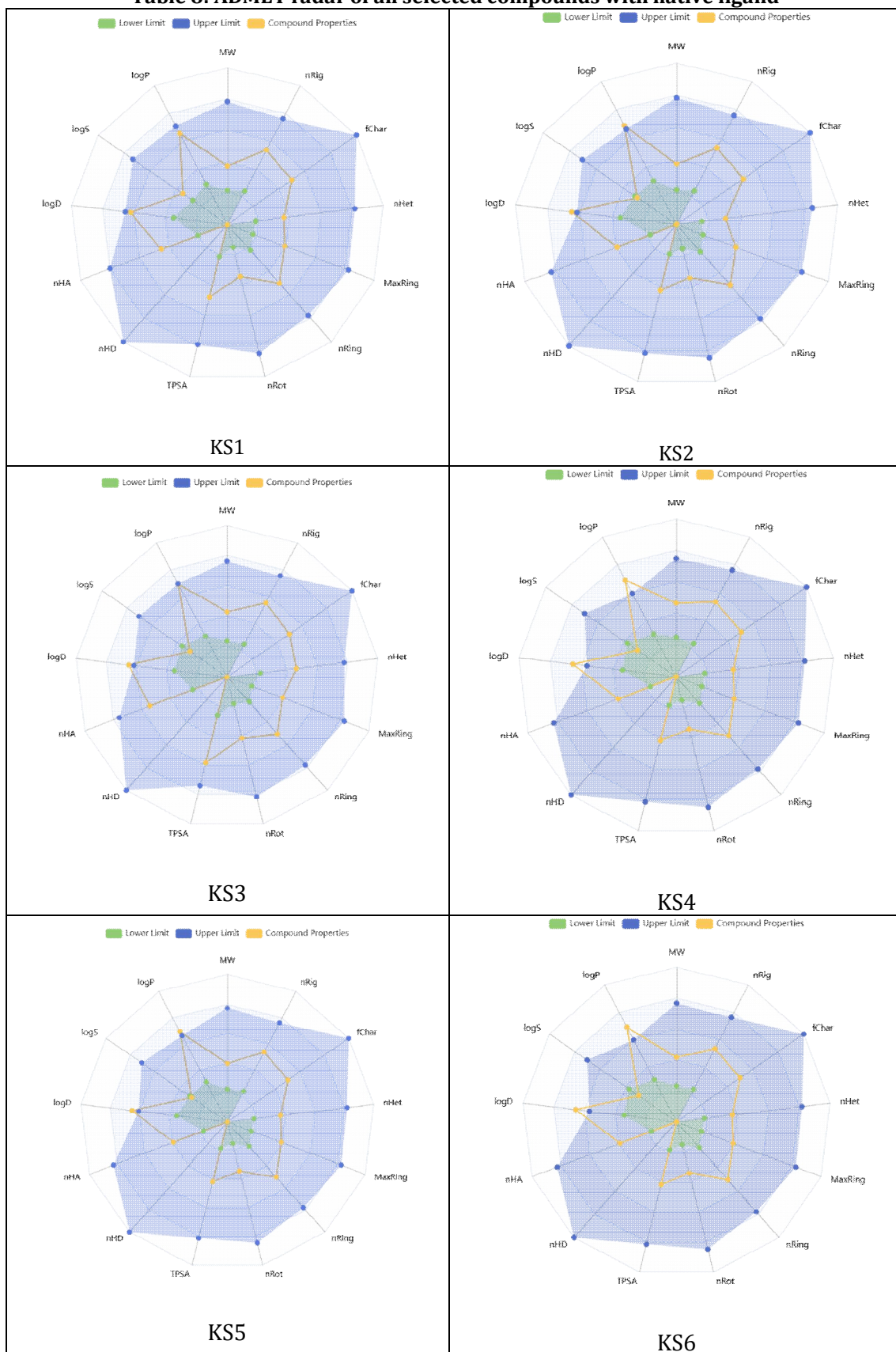
Compounds	Excretion		Toxicity									
	CL-plasma	T1/2	H-HT	DILI	Ames Toxicity	Rat Oral Acute Toxicity	FDA MDD	Skin Sensitization	Carcinogenicity	Eye Corrosion	Eye Irritation	Respiratory Toxicity
Native Ligand	0.893693	3.267466	0.022324	0.999996	0.256549	0.035818	0.913815	0.999907	0.030098	2.44E-07	0.09262	0.848013
KS1	6.781341	0.793149	0.84935	0.978481	0.86289	0.744342	0.64146	0.935041	0.967151	0.03202	0.981047	0.853517
KS2	6.146072	0.512671	0.823152	0.993327	0.748414	0.574378	0.588019	0.565684	0.933896	0.005744	0.9591	0.531096
KS3	5.185952	0.608881	0.859774	0.999571	0.965364	0.656937	0.682379	0.917769	0.955322	0.008899	0.989049	0.761102
KS4	4.965466	0.62925	0.776835	0.99703	0.5374	0.655523	0.795868	0.72091	0.931127	0.008353	0.969906	0.409675
KS5	6.091316	0.484462	0.827275	0.986619	0.783223	0.697393	0.731883	0.31249	0.94909	0.014274	0.960922	0.583791
KS6	5.885147	0.498479	0.819845	0.996584	0.605312	0.599907	0.595724	0.611196	0.920532	0.003496	0.892142	0.423924
KS7	6.180848	0.460763	0.824513	0.992206	0.734286	0.516888	0.577761	0.577191	0.93745	0.008472	0.963175	0.523427
KS8	7.466488	0.456604	0.765838	0.99287	0.778174	0.495652	0.577364	0.353147	0.945706	0.0077	0.95154	0.639433
KS9	6.826516	0.731752	0.791891	0.985699	0.725002	0.558406	0.66868	0.58642	0.936138	0.005447	0.97497	0.523096

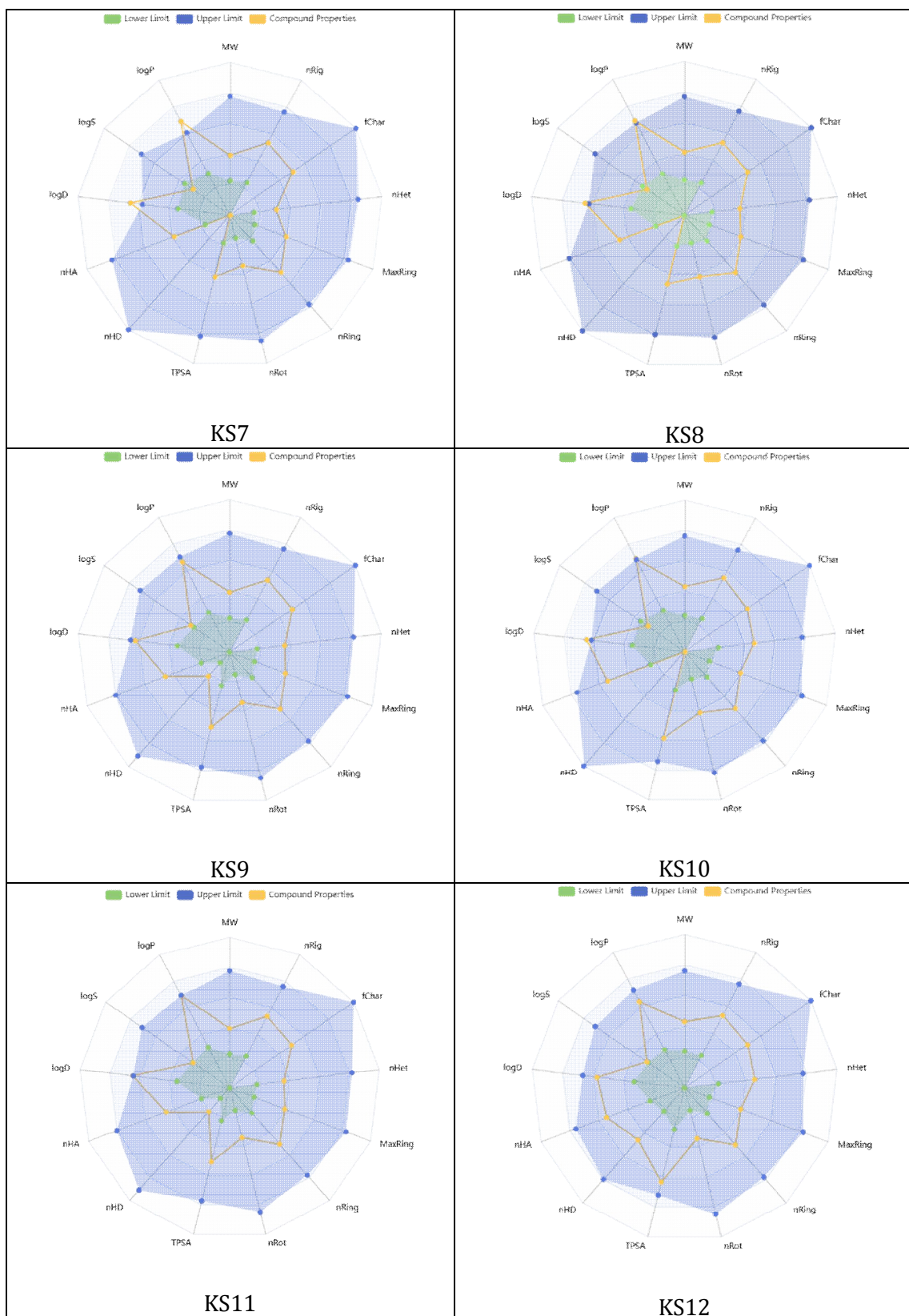
KS10	5.6527 82	0.5923 89	0.8479 82	0.9993 66	0.9409 42	0.6812 19	0.6626 68	0.8885 59	0.9375 27	0.0136 07	0.9873 44	0.7136 34
KS11	6.8105 33	0.5753 78	0.8056 11	0.9825 5	0.7524 77	0.5605 35	0.6615 94	0.5908 44	0.9337 51	0.0067 45	0.9724 23	0.5586 27
KS12	9.5701 57	1.1579 32	0.6377 23	0.9856 29	0.7428 63	0.5692 15	0.6692 07	0.9658 2	0.8431 89	0.0232 37	0.9840 06	0.4816 26
KS13	4.5298 71	0.8780 19	0.7486 94	0.9785 32	0.7323 49	0.5325 35	0.5807 92	0.5524 69	0.9214 49	0.0081 44	0.9629 62	0.6212 23
KS14	6.7106 25	0.4205 41	0.7630 05	0.9881 28	0.7183 09	0.5825 51	0.5223 65	0.3955 01	0.9283 44	0.0086 47	0.9507 76	0.5542 37
KS15	6.7793 79	0.5261 39	0.6974 54	0.9305 78	0.5841 1	0.5580 99	0.5531 55	0.2744 85	0.7267 25	0.0200 74	0.9562 33	0.5392 48
KS16	5.9050 82	0.4694 6	0.8264 21	0.9958 02	0.8375 21	0.6276 83	0.6438 76	0.3484 35	0.9438 55	0.0010 31	0.9365 39	0.6160 58
KS17	4.8416 94	0.7585 71	0.7288 09	0.9998 59	0.9877 29	0.7697 61	0.6647 87	0.9729 04	0.9370 91	0.0104 55	0.9915 54	0.8583 71
KS18	3.4539 85	0.7861 91	0.9014 19	0.9996 3	0.6214 06	0.5492 78	0.6324 46	0.1864 02	0.9319 27	0.0003 41	0.7396 42	0.2308 79
KS19	7.3783 26	0.4332 31	0.8055 25	0.9918 38	0.8816 15	0.6112 76	0.5232 93	0.4831 67	0.9818 61	0.0077 8	0.9901 21	0.8934 25
KS20	8.0965 8	0.5410 95	0.8776	0.9813 07	0.4825 91	0.6440 83	0.8395 43	0.2043 67	0.7790 2	0.0034 91	0.9506 85	0.7058 42

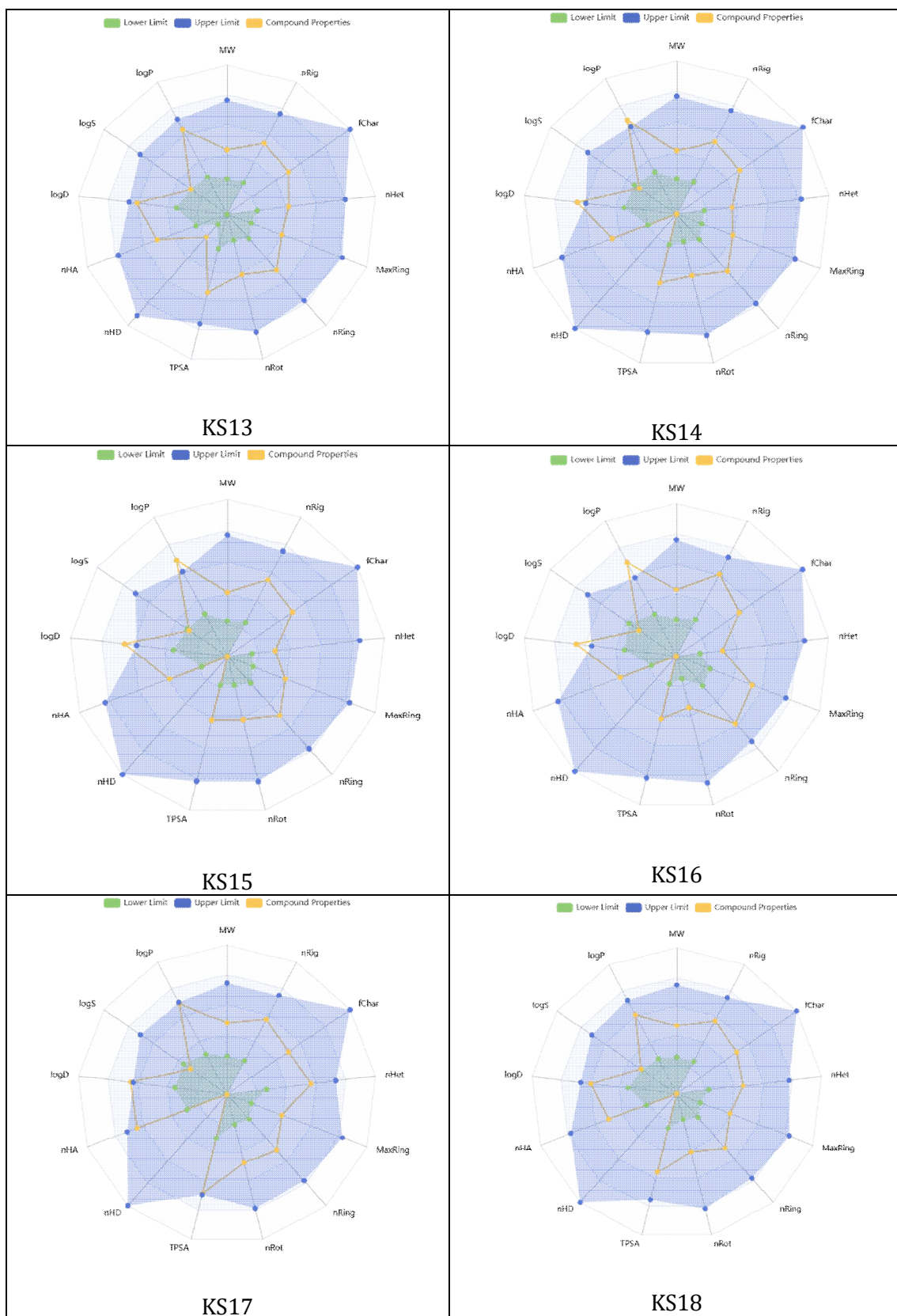
Table 7: Environmental toxicity profile of designed molecules

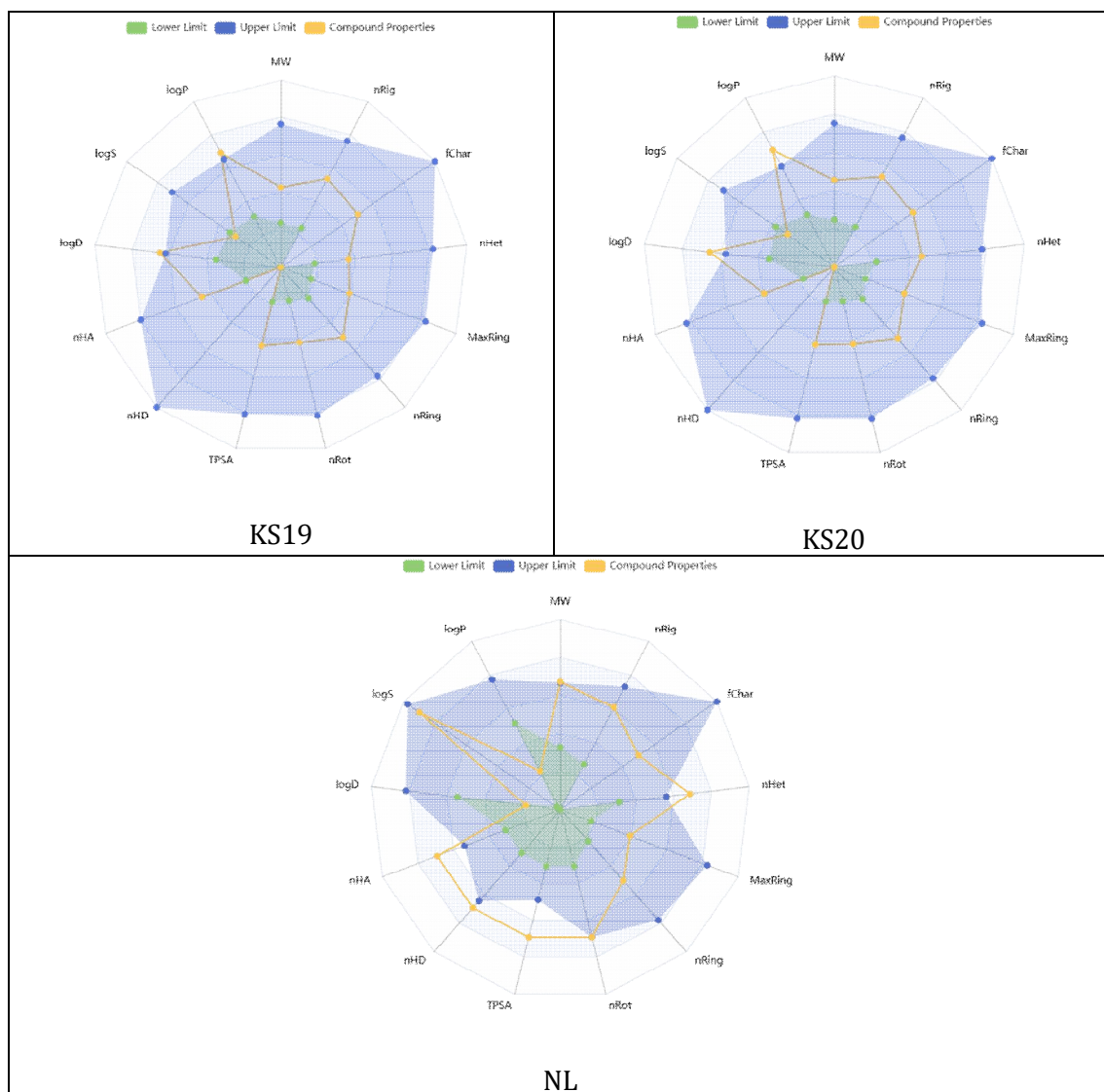
Compounds	BCF	IGC50	LC50FM	LC50DM
Native Ligand	-0.06387	2.210011	3.464563	4.224978
KS1	0.542693	3.110102	3.763392	4.179127
KS2	1.402684	3.899751	4.574273	4.745016
KS3	1.234551	3.904871	4.543917	4.854049
KS4	1.998658	4.077265	4.950452	5.501178
KS5	1.731145	3.672688	4.517727	4.8337
KS6	1.93845	4.174317	5.184766	5.665054
KS7	1.483676	3.882654	4.541303	4.689673
KS8	1.410315	3.947808	4.749408	5.155346
KS9	1.189976	3.820802	4.328552	4.564439
KS10	1.153493	3.813253	4.50124	4.730954
KS11	1.047295	3.691037	4.365068	4.565676
KS12	0.667819	3.354108	4.125006	4.318532
KS13	0.85866	3.520729	4.155304	4.450401
KS14	1.103495	3.726364	4.368136	4.521181
KS15	1.563883	3.868277	4.62389	4.813891
KS16	1.772676	4.24241	4.994954	4.929602
KS17	0.543772	4.121836	4.989141	4.84718
KS18	0.542329	3.192695	4.096134	4.442003
KS19	1.065749	3.667398	4.385997	4.693248
KS20	1.963538	3.81022	4.803782	5.347873

Table 8: ADMET radar of all selected compounds with native ligand









Molecular Docking

Molecular docking is a computational method used to predict the binding orientation and affinity of small molecules to their target proteins. This technique is widely employed in drug discovery and development processes to screen potential drug candidates and understand their interactions with biological targets. In this study, molecular docking was utilized to evaluate N-ethylidene-4-(furan-2-yl)oxazol-2-amine derivatives as potential inhibitors of MurG-glycosyltransferase, an enzyme crucial for bacterial cell wall biosynthesis. **Table 9** presents the docking scores and ligand energies of selected compounds (KS1-KS20) and the native ligand (NL). The docking score represents the binding affinity of the ligand to the target protein, with more negative values indicating stronger binding. The ligand energy reflects the internal energy of the compound in its docked conformation. Among the tested compounds, KS16 exhibited the most favorable docking score of -8.9 kcal/mol, surpassing the native ligand (-7.8 kcal/mol). This suggests that KS16 may have a higher binding affinity for the MurG-glycosyltransferase target compared to the native ligand. Other compounds showing promising docking scores include KS20 (-8.4 kcal/mol), KS10 (-7.9 kcal/mol), and KS15, KS7, KS3, and KS19 (all at -7.8 kcal/mol), which are comparable to or better than the native ligand. The ligand energies of the compounds vary, with KS18 having the highest value (779.02) and KS4 the lowest (461.5). However, it is important to note that the ligand energy alone does not determine the binding affinity, as evidenced by the lack of direct correlation between ligand energy and docking score.

Table 10 provides detailed information on the docking interactions of the most potent compounds (KS3, KS7, KS10, KS15, KS16, KS18, KS19, and KS20) and the native ligand (NL) with the target protein (1NLM). The interactions are categorized by amino acid residues, bond lengths, bond types, and bond categories.

The molecular docking analysis revealed detailed interactions between various compounds and the MurG-glycosyltransferase enzyme. NL, the reference compound, formed electrostatic and hydrogen bond interactions with GLU269, as well as hydrophobic interactions with PHE21 and ARG164. KS3 and KS7 exhibited similar binding patterns, forming salt bridges and attractive charge interactions with GLU269, along with pi-anion interactions. These compounds also engaged in hydrophobic interactions with ARG164, PHE21, PHE244, and other residues. KS10 showed a combination of electrostatic, hydrogen bond, and hydrophobic interactions, particularly with GLU269, PRO162, and PHE244. KS15, KS16, KS18, and KS19 all demonstrated strong interactions with GLU269 through salt bridges and attractive charge interactions, as well as pi-anion interactions. These compounds also formed various hydrophobic interactions with residues such as PHE21, PHE244, and VAL189. KS20 exhibited a unique interaction profile, forming hydrogen bonds and halogen interactions with ARG164 and PHE21, in addition to the common interactions with GLU269 and other residues. Overall, these compounds showed promising binding affinities and interaction patterns with the target enzyme, suggesting their potential as MurG-glycosyltransferase inhibitors for bacterial infections. **Table 11** illustrated the 2D and 3D poses of most potent compound and NL with MurG-glycosyltransferase enzyme (PDB ID: 1NLM).

Table 9: Docking score and ligand energy of selected compounds and NL.

Compound Code	Ligand Energy	Docking Score
	(Kcal/mol)	
NL	4837.82	-7.8
KS1	466.16	-6.7
KS2	462.2	-7.1
KS3	477.35	-7.8
KS4	461.5	-7.5
KS5	462.86	-7.4
KS6	461.48	-7.5
KS7	462.15	-7.8
KS8	477.19	-7.4
KS9	462.19	-7.2
KS10	483.24	-7.9
KS11	464.84	-7.5
KS12	477.55	-7.5
KS13	483.42	-7.5
KS14	556.58	-7.1
KS15	462.94	-7.8
KS16	510.73	-8.9
KS17	558.47	-7.7
KS18	779.02	-7.8
KS19	482.03	-7.8
KS20	470.84	-8.4

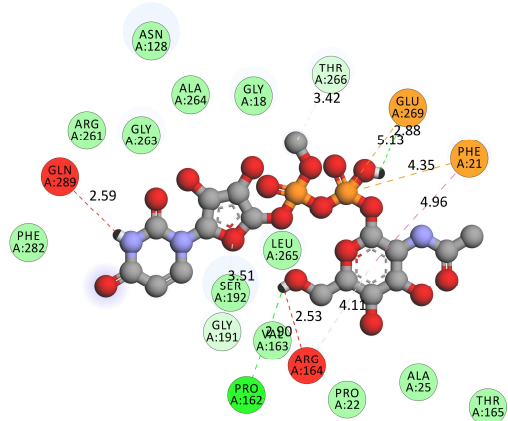
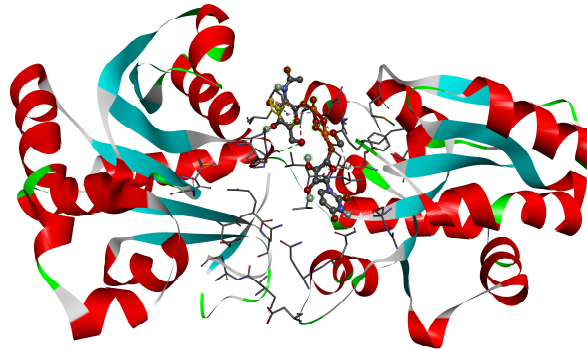
Table 10: Docking interactions of most potent compounds and NL with 1NLM

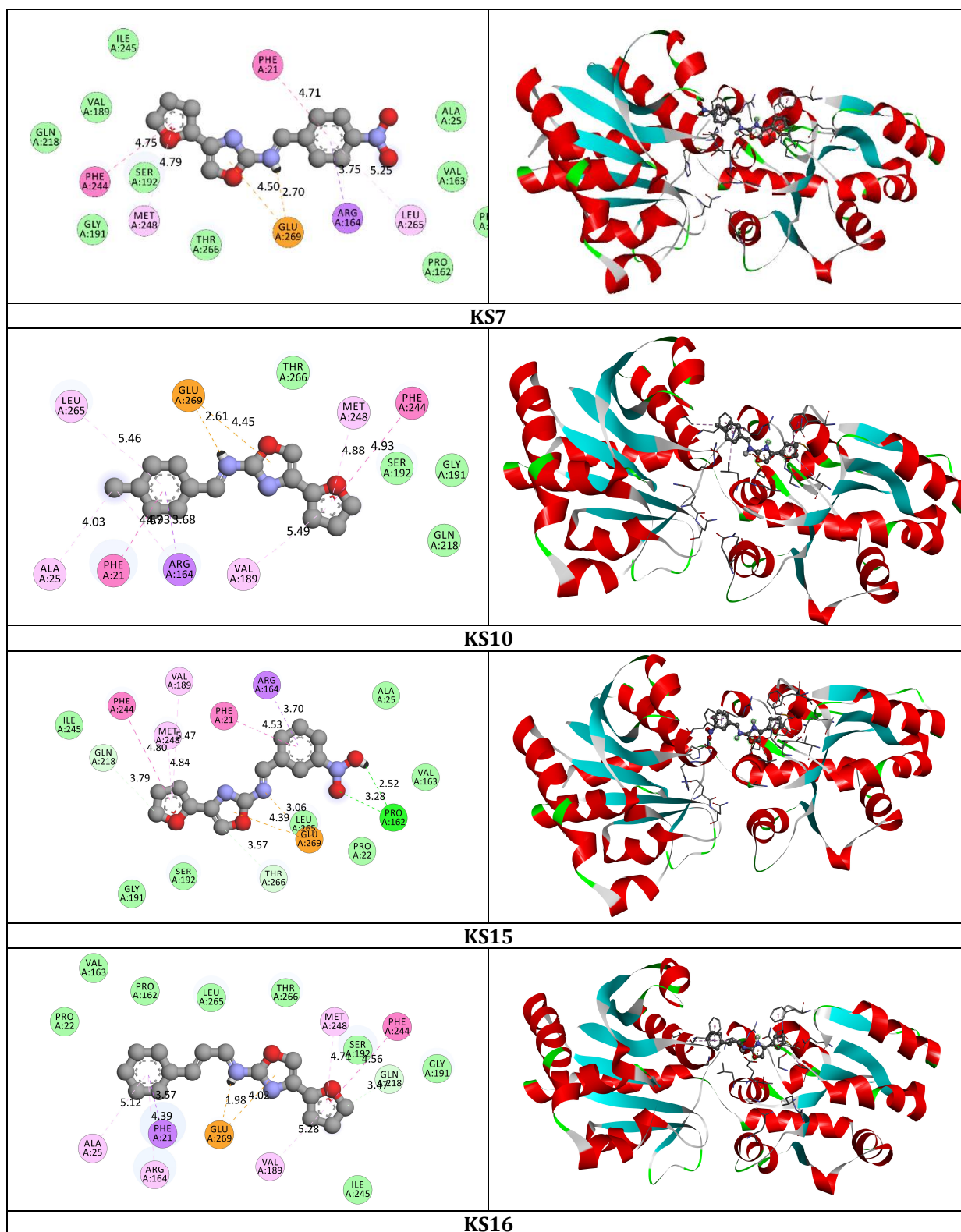
Amino acid residues	Bond Length	Bond Type	Bond Category
NL-1NLM			
GLU269	5.1333	Electrostatic	Attractive Charge
GLU269	2.88199	Hydrogen Bond	Conventional Hydrogen Bond
PRO162	2.90361		
THR266	3.42056		Carbon Hydrogen Bond
GLY191	3.51309		
PHE21	4.34668	Electrostatic	Pi-Cation
PHE21	4.96359	Hydrophobic	Pi-Pi Stacked
ARG164	4.11256		Pi-Alkyl
KS3			
GLU269	2.70038	Hydrogen Bond; Electrostatic	Salt Bridge; Attractive Charge
GLU269	4.50194	Electrostatic	Pi-Anion

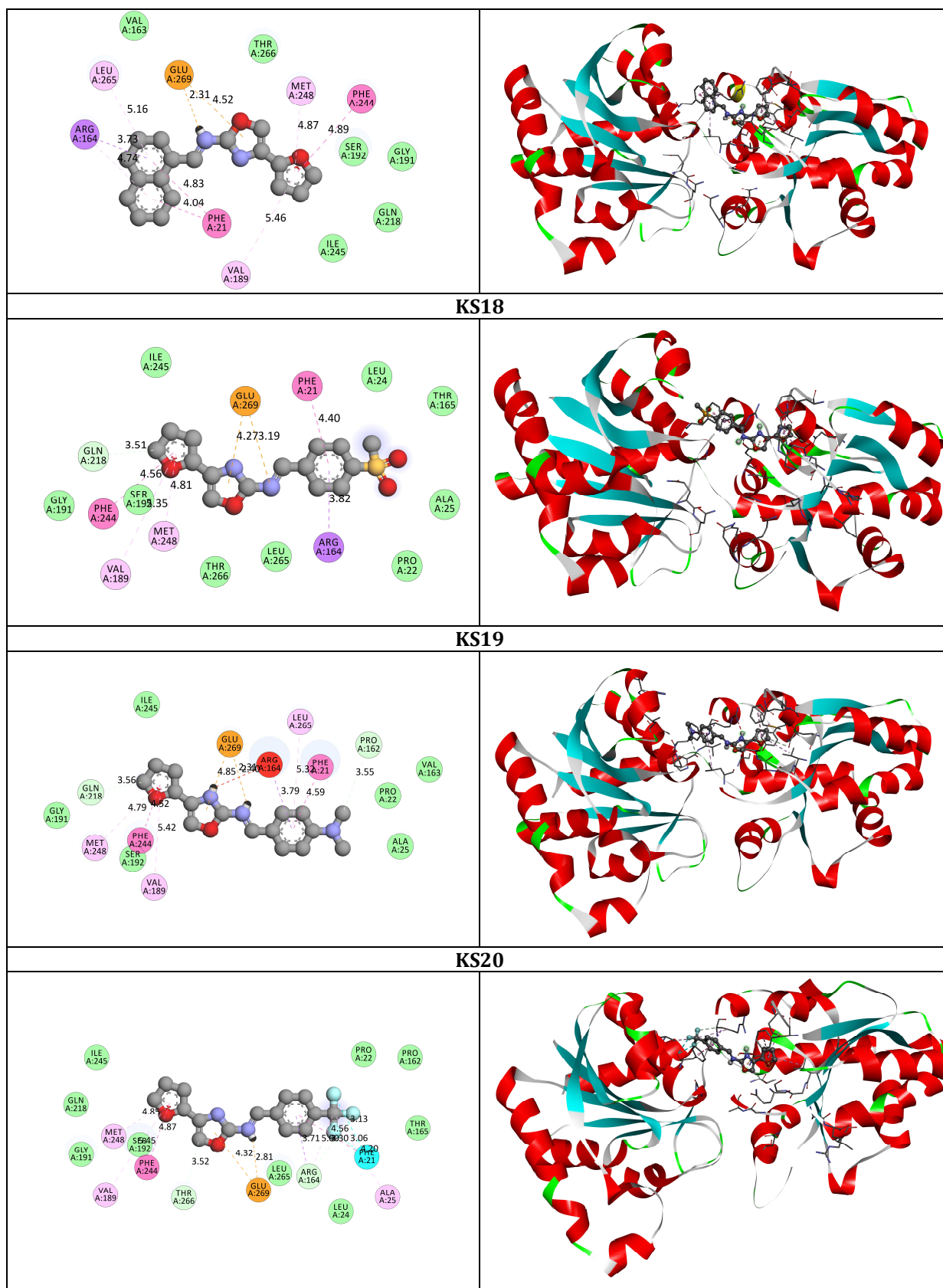
ARG164	3.74574	Hydrophobic	Pi-Sigma
PHE244	4.74686		Pi-Pi Stacked
PHE21	4.71103		
MET248	4.79498		Pi-Alkyl
LEU265	5.24707		
KS7			
GLU269	2.60614	Hydrogen Bond; Electrostatic	Salt Bridge; Attractive Charge
GLU269	4.44894	Electrostatic	Pi-Anion
ARG164	3.68444	Hydrophobic	Pi-Sigma
PHE21	4.66506		Pi-Pi Stacked
PHE244	4.92723		Alkyl
ALA25	4.02828		
ARG164	4.93188		
LEU265	5.46256		Pi-Alkyl
VAL189	5.4894		
MET248	4.88414		
KS10			
GLU269	3.06049	Electrostatic	Attractive Charge
PRO162	3.27605	Hydrogen Bond	Conventional Hydrogen Bond
PRO162	2.52232		Carbon Hydrogen Bond
THR266	3.57298		
GLN218	3.79359		
GLU269	4.39374	Electrostatic	Pi-Anion
ARG164	3.70347	Hydrophobic	Pi-Sigma
PHE244	4.80375		Pi-Pi Stacked
PHE21	4.53102		Pi-Alkyl
VAL189	5.47058		
MET248	4.83901		
KS15			
GLU269	1.97751	Hydrogen Bond; Electrostatic	Salt Bridge; Attractive Charge
GLN218	3.46855	Hydrogen Bond	Carbon Hydrogen Bond
GLU269	4.02264	Electrostatic	Pi-Anion
PHE21	3.5662	Hydrophobic	Pi-Sigma
PHE21	5.38628		Pi-Pi Stacked
PHE244	4.55914		Pi-Alkyl
:ALA25	5.1166		
ARG164	4.38726		
VAL189	5.27928		
MET248	4.70863		
KS16			
GLU269	2.30732	Hydrogen Bond; Electrostatic	Salt Bridge; Attractive Charge
GLU269	4.51738	Electrostatic	Pi-Anion
ARG164	3.7293	Hydrophobic	Pi-Sigma
PHE244	4.88661		Pi-Pi Stacked
PHE21	4.82901		Pi-Alkyl
PHE21	4.04135		
VAL189	5.45568		
MET248	4.87197		
LEU265	5.16123		
ARG164	4.74366		
KS18			
GLU269	3.18888	Electrostatic	Attractive Charge
GLN218	3.51191	Hydrogen Bond	Carbon Hvdrogen Bond

GLU269	4.26894	Electrostatic	Pi-Anion
ARG164	3.81627	Hydrophobic	Pi-Sigma
PHE244	4.55843		Pi-Pi Stacked
PHE21	4.4009		
VAL189	5.34947		Pi-Alkyl
MET248	4.80788		
KS19			
GLU269	2.30704	Hydrogen Bond; Electrostatic	Salt Bridge; Attractive Charge
GLN218	3.56026	Hydrogen Bond	Carbon Hydrogen Bond
PRO162	3.54758		
GLU269	4.85389	Electrostatic	Pi-Anion
ARG164	3.79236	Hydrophobic	Pi-Sigma
PHE244	4.51773		Pi-Pi Stacked
PHE21	4.59164		
VAL189	5.41988		Pi-Alkyl
MET248	4.79206		
LEU265	5.31676		
KS20			
GLU269	2.81014	Hydrogen Bond; Electrostatic	Salt Bridge; Attractive Charge
THR266	3.52339	Hydrogen Bond	Carbon Hydrogen Bond
ARG164	3.29576	Hydrogen Bond; Halogen	Carbon Hydrogen Bond; Halogen (Fluorine)
PHE21	3.12844	Halogen	Halogen (Fluorine)
PHE21	3.06425		
GLU269	4.32107	Electrostatic	Pi-Anion
ARG164	3.71083	Hydrophobic	Pi-Sigma
PHE244	4.86575		Pi-Pi Stacked
PHE21	4.55599		
ALA25	4.19897		Alkyl
ARG164	4.99538		
VAL189	5.44909		Pi-Alkyl
MET248	4.85212		

Table 11: 2D and 3D docking interactions of NL and most potent compounds.

2D Interactions	3D Interactions
NL	
	
KS3	





CONCLUSION

The present in silico investigation highlights the potential of N-ethylidene-4-(furan-2-yl)oxazol-2-amine derivatives as promising MurG-glycosyltransferase inhibitors for combating bacterial infections.

Antimicrobial resistance continues to present a major global challenge, and targeting MurG—a critical enzyme in peptidoglycan biosynthesis—offers an innovative therapeutic strategy, given its essential role in bacterial cell wall formation and absence in human pathways. ADMET profiling revealed that several designed derivatives exhibited improved drug-likeness, oral bioavailability, and pharmacokinetic properties compared to the native ligand, while also satisfying important medicinal chemistry rules. Compounds such as KS7, KS8, KS12, KS16, and KS20 demonstrated favorable absorption and distribution profiles, suggesting enhanced potential for systemic activity. Molecular docking further validated their inhibitory potential, with KS16 showing the most favorable docking score (-8.9 kcal/mol), followed by KS20, KS10, and KS15, all surpassing or matching the native ligand in binding affinity. Detailed interaction analyses confirmed that these compounds engaged in stable hydrogen bonding, electrostatic, and hydrophobic interactions with key active-site residues, particularly GLU269, ARG164, and PHE21. Collectively, the computational evidence underscores the potential of these derivatives as lead scaffolds for the development of next-generation antibacterial agents. However, further experimental validation is necessary to confirm their efficacy and safety for clinical applications.

References

1. Bessa G. (2023). Bacterial Infections. *Dermatology Public Heal Environ A Compr Textb Second Ed* [Internet]. ;183–202. Available from: https://link.springer.com/10.1007/978-3-031-13505-7_9
2. Jamal M, Ahmad W, Andleeb S, Jalil F, Imran M, Nawaz MA, et al. (2018). Bacterial biofilm and associated infections. *J Chinese Med Assoc.* 81(1):7–11.
3. Koutsoumanis K, Allende A, Álvarez-Ordóñez A, Bolton D, Bover-Cid S, Chemaly M, et al. (2021). Role played by the environment in the emergence and spread of antimicrobial resistance (AMR) through the food chain. *EFSA J.* ;19(6).
4. Lovering AL, Safadi SS, Strynadka NCJ. (2012). Structural perspective of peptidoglycan biosynthesis and assembly. *Annu Rev Biochem.* 81:451–78.
5. Garde S, Chodiseti PK, Reddy M. (2021). Peptidoglycan: Structure, Synthesis, and Regulation. *EcoSal Plus.* ;9(2). 890
6. Bouhss A, Trunkfield AE, Bugg TDH, Mengin-Lecreulx D. (2008). The biosynthesis of peptidoglycan lipid-linked intermediates. *FEMS Microbiol Rev.* 32(2):208–33.
7. Heijenoort J Van. (1994). Biosynthesis of the bacterial peptidoglycan unit. *New Compr Biochem.* 27(C):39–54.
8. Kim SJ, Chang J, Singh M. (2015). Peptidoglycan architecture of Gram-positive bacteria by solid-state NMR. *Biochim Biophys Acta - Biomembr.* 1848(1):350–62.
9. Galinier A, Delan-Forino C, Foulquier E, Lakhal H, Pompeo F. (2023). Recent Advances in Peptidoglycan Synthesis and Regulation in Bacteria. *Biomolecules.* 13(5). doi: 10.3390/biom13050720.
10. Vollmer W, Joris B, Charlier P, Foster S. (2008). Bacterial peptidoglycan (murein) hydrolases. *FEMS Microbiol Rev.* 32(2):259–86.
11. Vollmer W, Blanot D, De Pedro MA. (2008). Peptidoglycan structure and architecture. *FEMS Microbiol Rev.* ;32(2):149–67.
12. Trunkfield AE, Gurucha SS, Besra GS, Bugg TDH. (2010). Inhibition of *Escherichia coli* glycosyltransferase MurG and *Mycobacterium tuberculosis* Gal transferase by uridine-linked transition state mimics. *Bioorganic Med Chem.* 18(7):2651–63.
13. Mohammadi T, Karczmarek A, Crouvoisier M, Bouhss A, Mengin-Lecreulx D, Den Blaauwen T. (2007). The essential peptidoglycan glycosyltransferase MurG forms a complex with proteins involved in lateral envelope growth as well as with proteins involved in cell division in *Escherichia coli*. *Mol Microbiol.* 65(4):1106–21.
14. Hu Y, Helm JS, Chen L, Ginsberg C, Gross B, Kraybill B, et al. (2004). Identification of selective inhibitors for the glycosyltransferase murg via high-throughput screening. *Chem Biol.* 11(5):703–11.
15. Helm JS, Hu Y, Chen L, Gross B, Walker S. (2003). Identification of active-site inhibitors of MurG using a generalizable, high-throughput glycosyltransferase screen. *J Am Chem Soc.* 125(37):11168–9.
16. Laddomada F, Miyachiro MM, Jessop M, Patin D, Job V, Mengin-Lecreulx D, et al. (2019). The MurG glycosyltransferase provides an oligomeric scaffold for the cytoplasmic steps of peptidoglycan biosynthesis in the human pathogen *Bordetella pertussis*. *Sci Rep.* 2019;9(1). doi: 10.1038/s41598-019-40966-z.
17. Sadybekov A V., Katritch V. (2023). Computational approaches streamlining drug discovery. *Nature.* 616(7958):673–85.
18. Amamuddy OS, Veldman W, Manyumwa C, Khairallah A, Agajanian S, Oluyemi O, et al. (2020). Integrated computational approaches and tools for allosteric drug discovery. *Int J Mol Sci.* 21(3). doi: 10.3390/ijms21030847.
19. Siddiqui FA, Makhlofi R, Hojjati M, El-sayed MS, Eman K. (2025). Computational Exploration of Quinine and Mefloquine as Potential Anti-Malarial Agents. *J Pharm Sci Comput Chem.* 1(2):106–15.
20. Ahmed SA, Tabassum PS, Falak SA, Vikhar A, Ahmad D, Shaikh S. (2025). Molecular Docking and Network Pharmacology: Investigating *Vitis vinifera* Phytoconstituents as Multi-Target Therapeutic Agents against Breast Cancer. *J Pharm Sci Comput Chem* 2025 [Internet]. 1(2):116–34. Available from: <https://doi.org/10.48309/jpscc.2025.526713.1014>

21. Qiu Y, Qiu Z, He A, Xu J, Yang X, Zhang H, et al. (2023). A novel strategy for enhancing inhibitor tolerance of gram-positive bacteria through overexpression of the peptidoglycan synthesis genes *murG* and *mraY*. *Ind Crops Prod.* ;192.
22. Saxena S, Abdullah M, Sriram D, Guruprasad L. (2018). Discovery of novel inhibitors of mycobacterium tuberculosis *murg*: Homology modelling, structure based pharmacophore, molecular docking, and molecular dynamics simulations. *J Biomol Struct Dyn.*36(12):3184–98.
23. Tamboli AS, Tayade SD. (2025). In-Depth Investigation of Berberine and Tropane through Computational Screening as Possible DPP-IV inhibitors for the Treatment of T2DM. *J Pharm Sci Comput Chem* [Internet]. ;1(1):1–11. Available from: https://jpscc.samipubco.com/article_219587.html
24. Suryawanshi RM, Shimpi RB, Muralidharan V, Nemade LS, Gurugubelli S, Baig S, et al. (2025). ADME, Toxicity, Molecular Docking, Molecular Dynamics, Glucokinase activation, DPP-IV, α -amylase, and α -glucosidase Inhibition Assays of Mangiferin and Friedelin for Antidiabetic Potential. *Chem Biodivers* [Internet].23; Available from: <https://onlinelibrary.wiley.com/doi/10.1002/cbdv.202402738>
25. Fu L, Shi S, Yi J, Wang N, He Y, Wu Z, et al. (2024). ADMETlab 3.0: an updated comprehensive online ADMET prediction platform enhanced with broader coverage, improved performance, API functionality and decision support. *Nucleic Acids Res.* 52(W1):W422–31.
26. Lagorce D, Douguet D, Miteva MA, Villoutreix BO. (2017). Computational analysis of calculated physicochemical and ADMET properties of protein-protein interaction inhibitors. *Sci Rep.* 7.
27. Ezugwu JA, Okoro UC, Ezeokonkwo MA, Hariprasad KS, Rudrapal M, Gogoi N, et al. (2024). Design, Synthesis, Molecular Docking, Drug-Likeness/ADMET and Molecular Dynamics Studies of Thiazolyl Benzenesulfonamide Carboxylates as Antimalarial Agents. *Chem Africa.* 7(5):2353–68.
28. Cheng F, Li W, Liu G, Tang Y. (2013). In Silico ADMET Prediction: Recent Advances, Current Challenges and Future Trends. *Curr Top Med Chem.*13(11):1273–89.
29. Thenmozhi V, Santhanakumar M, Venkateshan N, Prasanthi G, Sarangi RR, Nayak SK, et al. (2025). Investigation of N-(5-nitrothiazol-2-yl)-2-((4-oxo-3,4-Dihydroquinazolin-2-yl) Thio) Acetamide Derivatives as Potential EGFR Kinase Inhibitors. *Adv J Chem Sect A.* 8(8):1398–430.
30. Sonwane G, Kale M, Khan S. (2022). Rationale Design, Synthesis, Cytotoxicity Evaluation and Molecular Docking Studies of 3-Chloro-4-aryl-1-(phenazin-7-yl) Azetidin-2-ones Analogues. *Indian J Heterocycl Chem.* ;32(3):393–9.
31. Unnisa A, Kunduru RD, Jandrajupalli SB, Elamine BA, Banu H, Baratam A, et al. (2023). Molecular Docking and in vitro Enzyme Assay of Bioactive Compound Isolated from *Rhus tripartite* Collected from Hail Region of Saudi Arabia as Potential Anti-Diabetic Agent. *Indian J Pharm Educ Res.* ;57(2). 90-94

Copyright: © 2025 Society of Education. This is an open access article distributed under the Creative Commons Attribution License, which permits unrestricted use, distribution, and reproduction in any medium, provided the original work is properly cited.